New spectral imaging biomarkers for sepsis and mortality in intensive care

Silvia Seidlitz^{1,2,3,4*}, Katharina Hölzl^{1,5}, Ayca von Garrel^{1,5}, Jan Sellner^{1,2,3,4}, Stephan Katzenschlager⁵, Tobias Hölle⁵, Dania Fischer⁵, Maik von der Forst⁵, Felix C. F. Schmitt⁵, Markus A. Weigand^{5†}, Lena Maier-Hein^{1,2,3,4,6*†}, Maximilian Dietrich^{5†}

⁶Medical Faculty, Heidelberg University, Heidelberg, Germany.

*Corresponding author(s). E-mail(s): s.seidlitz@dkfz-heidelberg.de; l.maier-hein@dkfz-heidelberg.de; †These authors contributed equally to this work.

Abstract

With sepsis remaining a leading cause of mortality, early identification of septic patients and those at high risk of death is a challenge of high socioeconomic importance. The driving hypothesis of this study was that hyperspectral imaging (HSI) could provide novel biomarkers for sepsis diagnosis and treatment management due to its potential to monitor microcirculatory alterations. We conducted a comprehensive study involving HSI data of the palm and fingers from more than 480 patients on the day of their intensive care unit (ICU) admission. The findings demonstrate that HSI measurements can predict sepsis with an area under the receiver operating characteristic curve (AUROC) of 0.80 (95% confidence interval (CI) [0.76; 0.84]) and mortality with an AUROC of 0.72 (95% CI [0.65; 0.79]). The predictive performance improves substantially when additional clinical data is incorporated, leading to an AUROC of up to 0.94 (95% CI [0.92; 0.96]) for sepsis and 0.84 (95% CI [0.78; 0.89]) for mortality. We conclude that HSI presents novel imaging biomarkers for the rapid, non-invasive prediction of sepsis and mortality, suggesting its potential as an important modality for guiding diagnosis and treatment.

Keywords: hyperspectral imaging, functional imaging, deep learning, microcirculation monitoring, sepsis diagnosis, mortality prediction, intensive care

^{1*}Division of Intelligent Medical Systems (IMSY), German Cancer Research Center (DKFZ), Heidelberg, Germany.

²Helmholtz Information and Data Science School for Health, Heidelberg/Karlsruhe, Germany.

³Faculty of Mathematics and Computer Science, Heidelberg University, Heidelberg, Germany.

⁴National Center for Tumor Diseases (NCT), NCT Heidelberg, a partnership between DKFZ and university medical center Heidelberg.

⁵Heidelberg University, Medical Faculty, Department of Anesthesiology, Heidelberg University Hospital, Heidelberg, Germany.

1 Main

Sepsis is defined as a life-threatening organ dysfunction resulting from a dysregulated host response to infection [1]. It represents a leading cause of mortality and critical illness worldwide, accounting for 19.7% of global deaths in 2017 [2]. As the clinical diagnosis of sepsis relies on the presence of organ dysfunction, only patients in advanced stages of the sepsis syndrome are typically identified [1]. The resulting delay in sepsis diagnosis is critical as the risk of mortality escalates with each hour of treatment delay due to irreversible organ damage [3]. Conversely, patients incorrectly presumed to have sepsis are often treated unnecessarily with antibiotics, which contributes to the development of multidrug-resistant organisms [4]. A critical aspect of sepsis management is the early and accurate diagnosis prior to the onset of persistent organ dysfunction. This task is complicated by the nonspecific signs and symptoms of the sepsis syndrome, along with the complex, heterogeneous, and not yet fully understood sepsis pathophysiology [5]. A particular challenge lies in distinguishing between septic and non-septic critically ill patients in the intensive care unit (ICU) due to the higher baseline illness severity and frequent organ failure from both septic and non-septic inflammation [6].

Beyond the early identification of septic patients, the early and accurate identification of ICU patients at high risk of death is crucial. This is because it can substantially improve individual patient outcomes by enabling the timely implementation of appropriate interventions, thereby enhancing patient care [7]. Moreover, it has the potential to improve the overall efficiency and effectiveness of critical care delivery. This could be achieved through optimised allocation of limited resources, informed decisions regarding palliative care, and a deeper understanding of the factors that influence patient outcomes [7, 8].

Over the past decades, considerable research efforts have focused on identifying biomarkers for sepsis diagnosis and mortality prediction, with over 250 molecules proposed as potential diagnostic or prognostic markers. However, to date, no single biomarker has demonstrated outstanding sensitivity and specificity for detecting sepsis and predicting mortality [9].

More recently, studies have investigated the use of machine learning to predict sepsis and mortality based on high-dimensional clinical data extracted from electronic health records (EHRs) [10]. The random forest model has emerged as the most commonly employed machine learning model in these studies [11]. A 2020 meta-analysis, which included 28 papers presenting 130 models, reported area under the receiver operating characteristic curve (AUROC) values ranging from 0.68 to 0.99 for predicting sepsis up to 48 hours before onset [12, 13]. Despite the promising performance metrics reported in research studies, the clinical translation of EHR-based sepsis and mortality prediction models faces substantial challenges. EHR data, which is primarily collected for the purpose of clinical documentation and billing, lacks standardisation, is incomplete and inaccurate and contains inherent biases (e.g., association between the frequency of measurement and the severity of the disease, sample selection biases) [14]. These factors can lead to limited generalizability on external datasets, as demonstrated for several EHR-based sepsis prediction models [15, 16]. Furthermore, while EHR adoption is widespread in high-income countries, it lags in low- and middle-income countries (LMICs), where 85% of sepsis cases occur [2]. This disparity is due to limited availability of expensive monitoring equipment, restricted laboratory access, insufficient technical support, inadequate infrastructure, and a lack of proper training and implementation frameworks [17].

In recent years, the monitoring of microcirculatory alterations in critically ill patients has gained attention [18]. Due to the common decoupling of microcirculation and systemic haemodynamics in sepsis, systemic haemodynamic parameters (e.g., blood pressure, cardiac output) are insufficient for effectively monitoring microcirculation [18, 19]. Imaging methods such as sublingual microscopy, laser Doppler flowmetry, laser speckle contrast imaging, near-infrared spectroscopy, and hyperspectral imaging (HSI) have revealed that microcirculatory dysfunction in sepsis is characterised by reduced capillary density and increased heterogeneity in microperfusion, leading to local zones of hypoxia [20, 21]. This dysfunction develops early during sepsis [19] and is a key driver of

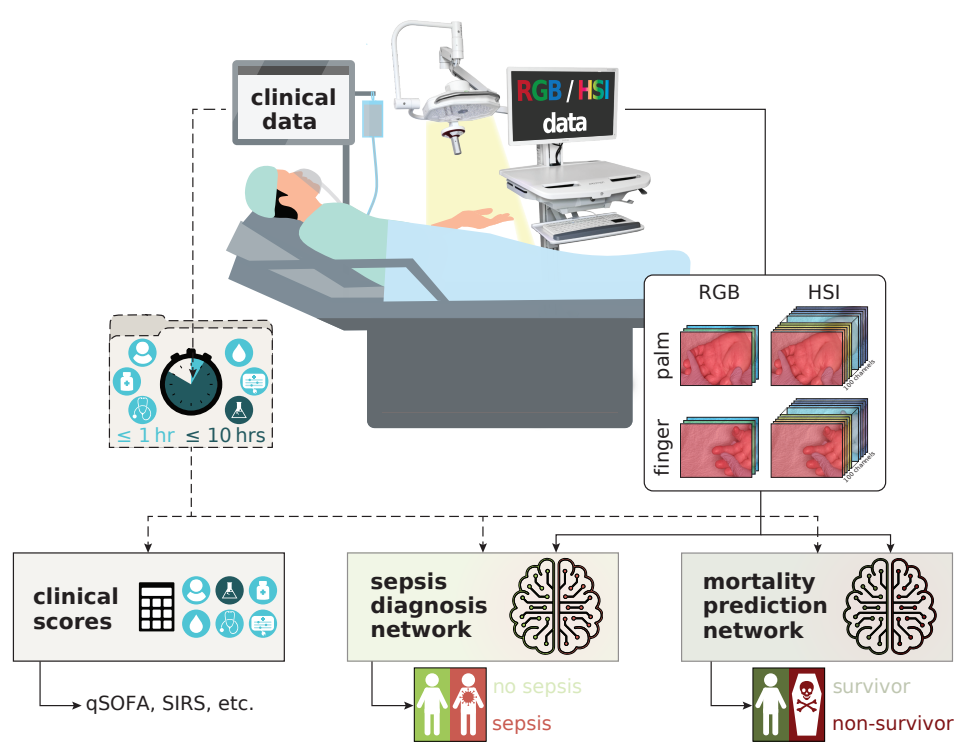


Fig. 1 We explore hyperspectral imaging (HSI) for automated, non-invasive and rapid sepsis diagnosis and mortality prediction. In a prospective study of over 480 intensive care unit (ICU) patients, we collected HSI and redgreen-blue (RGB) images of the palm and annular finger, and clinical data. Deep learning accurately predicts sepsis and mortality from HSI data, with improved performance when combined with clinical data. Our method outperforms widely used clinical biomarkers and scores such as the quick Sequential Organ Failure Assessment (qSOFA) score and the Systemic Inflammatory Response Syndrome (SIRS) criteria.

organ failure, being associated with poor outcomes [22, 23].

We hypothesise that HSI could serve as an imaging biomarker for automated sepsis diagnosis and mortality prediction in ICU patients by monitoring microcirculatory dysfunction and edema formation. The key strengths of HSI include its mobile, non-invasive, rapid, objective, costeffective, and standardised assessments. Unlike other imaging modalities capable of monitoring microcirculation, medical device-graded HSI systems have begun to emerge, paving the way for HSI to become a routine clinical tool [18, 24]. Previous research has identified patterns in functional parameters derived from HSI when comparing septic patients to healthy volunteers [24, 25], as well as septic non-survivors to survivors [26]. While recent initial work on HSI-based sepsis diagnosis performed by ourselves [27] and others in parallel [28] showed promising early results, all studies conducted so far come with the major limitation that sepsis patients were compared to healthy

volunteers or selectively chosen cohorts, such as patients undergoing pancreatic surgeries. Hence, the proposed algorithms are at high risk of short-cut learning due to confounders such as substantial age gaps and differences in comorbidities and therapies between septic patients and non-septic controls [27]. Consequently, they are unlikely to generalise well to realistic clinical applications, such as automated sepsis diagnosis in critically ill ICU patients.

In summary, despite extensive research efforts, robust biomarkers for early sepsis diagnosis and mortality prediction are still lacking. In this article, we close this important gap by presenting the first analysis of deep learning-based HSI analysis for automated, non-invasive, and rapid diagnosis of sepsis and prediction of mortality among ICU patients. Based on a prospective study involving over 480 patients, representing, to the best of our knowledge, the largest medical HSI dataset to date, we investigate the following research questions (cf. Figure 1):

- Is an automated, non-invasive and rapid diagnosis of sepsis and prediction of mortality among ICU patients feasible with deep learning-based HSI analysis? What is the optimal measurement site and modality?
- 2. Can we further boost the diagnostic and predictive performance by adding structured clinical data?
- 3. Does our method outperform widely available clinical scores and biomarkers?

2 Results

Using the medical device-graded HSI system Tivita[®] 2.0 Surgery Edition (Diaspective Vision, Am Salzhaff, Germany), we collected HSI data and corresponding red-green-blue (RGB) images from the skin of all patients admitted to the interdisciplinary surgical ICU at the University Hospital Heidelberg over one year. This resulted in data from 308 non-septic and 129 septic patients. Successful follow-up to determine the survival status at 30 days of inclusion could be achieved for 483 patients, including 68 non-survivors (14%). The mortality rate was 27% (35/129) for patients diagnosed with sepsis at the time of admission, compared to a lower rate of 6% (18/308) for those without sepsis at admission. The palm and annular finger were chosen as measurement sites due to their easy accessibility and low melanin content.

2.1 HSI can rapidly and non-invasively diagnose sepsis and predict mortality

As shown in Figure 2, deep learning-based diagnosis of sepsis from the palm was achievable with an AUROC of 0.80~(95~% confidence interval (CI) [0.76;~0.84]), while the finger measurements yielded an AUROC of 0.72~(95~% CI [0.67;~0.77]). Also for mortality prediction, the palm measurement site yielded better classification performance (AUROC 0.72~(95~% CI [0.65;~0.79])), compared to the finger measurements (AUROC 0.65~(95~% CI [0.58;~0.73])). HSI demonstrated superior diagnostic performance compared to RGB imaging, with up to a 20~% improvement.

2.2 Septic patients and non-survivors have decreased tissue oxygen saturation at increased tissue water and haemoglobin content

HSI captures tissue reflectance spectra, which are affected by chromophores like haemoglobin and water within the tissue. Consequently, functional parameters such as oxygen saturation, perfusion, haemoglobin content, and water content can be approximated from HSI data [29, 30].

According to the formulas in [29], tissue oxygen saturation, perfusion index, haemoglobin index and water index were computed, and distributions for septic and non-septic patients, as well as survivors and non-survivors are shown in Figure 3. In septic patients, oxygen saturation was significantly lower compared to non-septic patients $(p = 7.1 \cdot 10^{-4})$, while haemoglobin and water index were significantly higher ($p = 6.2 \cdot 10^{-5}$ and $p = 4.5 \cdot 10^{-10}$, respectively). The perfusion index did not show a significant difference (p = $1.1 \cdot 10^{-1}$). In non-survivors, perfusion index and oxygen saturation were significantly lower (p = $2.5 \cdot 10^{-3}$ and $p = 6.8 \cdot 10^{-4}$, respectively) compared to survivors, and haemoglobin and water index were significantly higher $(p = 6.0 \cdot 10^{-4})$ and $p = 7.0 \cdot 10^{-5}$, respectively). More details on the statistical tests are available in Table A1.

2.3 Structured clinical data boosts the classification performance

Structured clinical data were collected alongside the HSI data, including demographics, vital signs, blood gas analysis measurements, therapy details (usage of organ replacement therapies, ventilation parameters, and dose of administered vasopressors and inotropes), and laboratory results. A total of 45 clinical parameters were recorded, with 33 usually available within one hour of admission and the 12 laboratory parameters usually available within ten hours of admission. Descriptive statistics of the clinical parameters are available in Table A2 and Table A3.

Incorporating clinical data available within the first hour of ICU admission alongside HSI data of the palm in the HSI + clinical data model improved sepsis diagnosis performance from an AUROC of 0.80~(95~%~CI~[0.76;0.84]) to 0.89~(95~%~CI~[0.76;0.84])

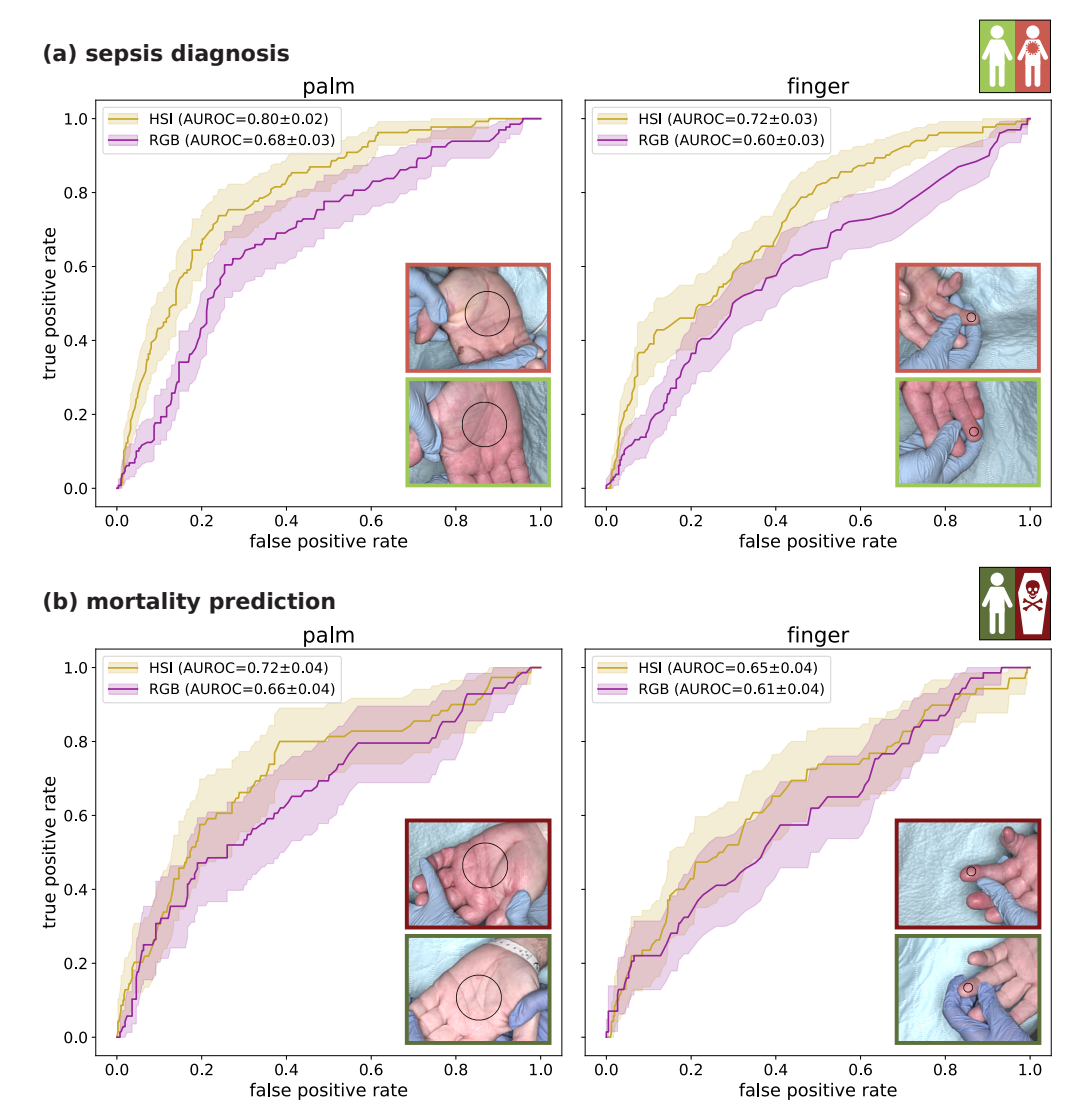


Fig. 2 Hyperspectral imaging (HSI) can rapidly and non-invasively diagnose sepsis and predict mortality. Receiver operating characteristics (ROCs) are shown for sepsis diagnosis (a) and mortality prediction (b) models based on HSI (gold) and red-green-blue (RGB) (violet) data of the palm (left) and annular finger (right). The shaded areas denote the 95 % confidence interval across 1000 bootstrap samples, and mean and standard deviation of the area under the receiver operating characteristic curve (AUROC) are reported in the legend. Sample images of a septic (light red box) and non-septic (light green box) patient, as well as a survivor (dark green) and non-survivor (dark red) are included on the bottom right, with the circle denoting the annotated skin region.

CI [0.86; 0.92]) (cf. Figure 4). The performance further increased to 0.94 (95% CI [0.92; 0.96]) when laboratory values, available within ten hours post-admission, were also included. Although a random forest model using comprehensive clinical data alone, referred to as clinical data model, performed slightly better on the full set of clinical data, combining HSI with clinical data performed substantially better when only limited

clinical data was available, a common scenario in emergency settings, outpatient health care and LMICs. Sequential incorporation of clinical data based on the feature importance of the clinical data model (cf. Figure 4) revealed that the HSI + clinical data model already achieved an AUROC of 0.87 (95% CI [0.83; 0.90]) by combining a single clinical parameter immediately

(a) sepsis diagnosis cohort water index oxygen saturation perfusion index haemoglobin index 0.8 0.6 0.8 0.7 index value [a.u.] 0.0 0.0 4 0.0 4 0.5 0.6 0.7 0.4 0.3 0.4 0.6 0.2 0.2 0.1 0.5 0.3 0.0 sepsis no sepsis no sepsis sepsis no sepsis sepsis no sepsis sepsis sepsis status sepsis status sepsis status sepsis status (b) mortality prediction cohort oxygen saturation perfusion index haemoglobin index water index 0.8 0.8 0.8 index value [a.u.] 0.5 0.7 0.6 0.4 0.7 0.6 0.3 0.4 0.5 0.6 0.2 0.4 0.2 0.1 0.5 0.3 non-survivor non-survivo non-survivor survivor survivor survivor non-survivor survivor

Fig. 3 Septic patients and non-survivors possess significantly lower tissue oxygen saturation, and higher tissue haemoglobin and water index. The subfigures show the distribution of the functional parameters oxygen saturation, perfusion index, haemoglobin index and water index, derived from hyperspectral imaging (HSI) palm measurements, for septic and non-septic patients (a), and survivors and non-survivors (b). The boxes denote the quartiles of the distribution with the whiskers extending up to 1.5 times the interquartile range, and the median and mean drawn as solid and dashed lines, respectively. Each dot represents one patient.

survival status

survival status

available at bedside, namely the administered noradrenaline dose, with HSI data.

survival status

Combining HSI with clinical data also boosted the mortality prediction performance. The AUROC improved from 0.72 (95 % CI [0.65; [0.79]) to [0.83] (95 % CI [0.77; 0.88]) when including clinical data available within the first hour of admission, and further to 0.84 (95 % CI [0.78; 0.89) when incorporating clinical data from the first ten hours of admission. The HSI + clinical data model consistently performed better than the clinical data model across all clinical data sets, with the greatest advantage observed when only limited clinical data was available. The three most important clinical data available within one hour from admission were lactate, pH and noradrenaline dose, which achieved an AUROC of 0.80 (95% CI [0.73; 0.85]) in combination with HSI data.

2.4 Our HSI biomarker surpasses clinical biomarkers and scores for sepsis diagnosis and mortality prediction

survival status

We compared our HSI + clinical data models with commonly used clinical biomarkers and scores for sepsis diagnosis and mortality prediction.

Rapidly available bedside scores for sepsis diagnosis include the skin mottling score (SMS) [31] and capillary refill time (CRT) [32], both of which depend on visual skin assessment. Additionally, we compared our models to the quick Sequential Organ Failure Assessment (qSOFA) score [1] and the National Early Warning Score (NEWS) [33], which are based on vital signs and cognitive function. Among the biomarkers and scores available within ten hours from admission,

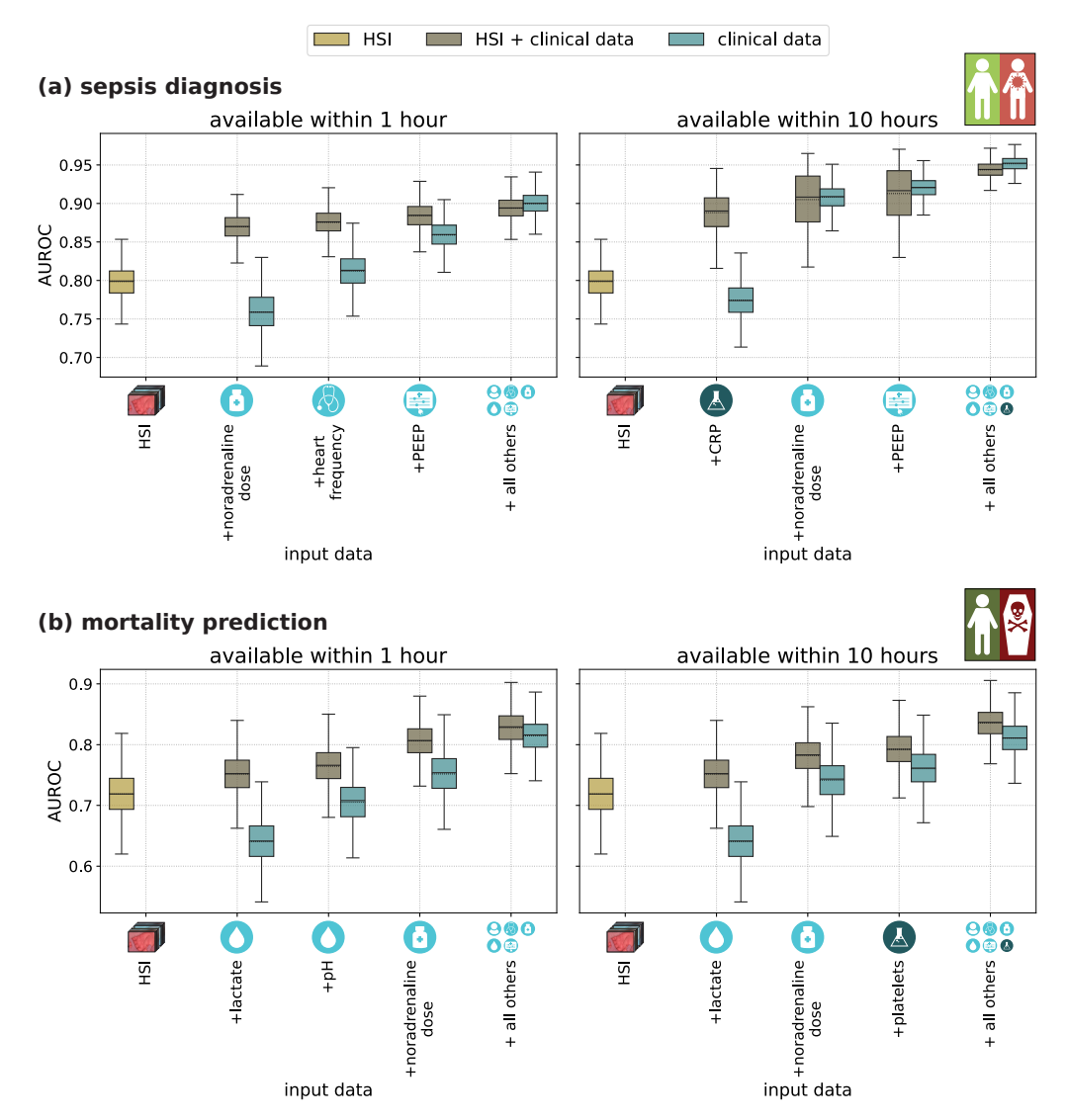


Fig. 4 Adding clinical data boosts the sepsis diagnosis and mortality prediction performance. The performance of sepsis diagnosis (a) and mortality prediction (b) using hyperspectral imaging (HSI) data (gold), a combination of HSI and clinical data (bronze), and clinical data alone (blue) is shown, categorised by data availability within one hour (left) and ten hours (right) from admission to the intensive care unit. Within the subplots, HSI-based classification is compared to sequentially adding the first, second and third most important clinical data, derived from the clinical data model, as well as using the complete set of available clinical data (from left to right). Each boxplot represents the quartiles of the area under the receiver operating characteristic curve (AUROC) distribution across 1000 bootstrap samples, with whiskers extending up to 1.5 times the interquartile range. The median and mean are drawn as solid and dashed lines, respectively.

we compared our models against the inflammatory biomarkers procalcitonin (PCT) and C-reactive protein (CRP), as well as the Systemic Inflammatory Response Syndrome (SIRS) criteria which were formerly used for sepsis diagnosis [34].

Commonly used clinical biomarkers and scores for assessing disease severity and risk of mortality include the vasoactive inotropic score (VIS) [35], the Sequential Organ Failure Assessment (SOFA) score [1], and the Acute Physiology and Chronic Health Evaluation (APACHE) II score [36]. The VIS, which quantifies haemodynamic support based on vasopressor and inotrope doses, is available within one hour of admission. Within

ten hours, the SOFA score, assessing organ dysfunction, and the APACHE II score, measuring disease severity, are available. These scores are derived from various vital signs, laboratory parameters, and patient and therapy characteristics, typically using the most abnormal readings within the last 24 hours. To compare our HSI+clinical data models with clinical scores, we employed modified versions of the SOFA and APACHE II scores, which were based on the most current data rather than the worst values over 24 hours, ensuring that values were available on the day of admission.

As shown in Figure 5, our HSI + clinical data models outperformed all clinical biomarkers and scores for both sepsis diagnosis and mortality prediction.

3 Discussion

In this study, we are the first to demonstrate that automated, non-invasive, and rapid diagnosis of sepsis and prediction of mortality among ICU patients is feasible using deep learning-based HSI analysis. Based on the — to the best of our knowledge — largest HSI patient cohort to date, we derived the following key findings:

- HSI biomarker: Both sepsis and mortality can be predicted from HSI data with high accuracy using deep learning. Septic patients and nonsurvivors have significantly lower tissue oxygen saturation, and higher tissue haemoglobin and water content than non-septic patients and non-survivors. Predictions from HSI measurements of the palm are superior to those from the annular finger.
- 2. Combination with structured clinical data: Incorporating structured clinical data enhances classification performance, yielding an AUROC of up to 0.94 and 0.84 for sepsis diagnosis and mortality prediction, respectively.
- Comparison to clinical biomarkers and scores: Our HSI + clinical data models outperform widely used clinical biomarkers and scores that were suggested for sepsis diagnosis and mortality prediction.

3.1 Strengths and limitations of our HSI biomarkers

We believe the primary strengths of our HSIbased sepsis diagnosis and mortality prediction are its objectivity, non-invasiveness, cost-effectiveness and speed, as predictions can be obtained from a single HSI cube acquired at the bedside within seconds. Additionally, HSI systems enable mobile measurements, and could thus be performed in various hospital wards, such as the emergency department, or even in ambulances. Although HSI systems are not yet widely used clinically, they have evolved rapidly over the past two decades from custom research prototypes to medically certified systems, like the one used in this study [37]. Manufacturers such as imec (Leuven, Belgium) and HAIC (Hanover, Germany) are currently focusing on developing more compact, real-time HSI devices and scaling production to achieve high-volume, low-cost availability.

We acknowledge that our classification models based on HSI data alone may not be sufficiently accurate as a standalone diagnostic and prognostic tool. However, we believe our HSI biomarker has high potential as a pre-screening tool to identify patients for which time-consuming and costly tests (e.g. laboratory measurements) and extensive monitoring should be performed. This is particularly advantageous in resource-limited settings, such as LMICs, where approximately half of critical care interventions are delivered outside of the ICU [38], and in situations requiring immediate decisions, such as emergency treatment.

We showed that substantial performance improvements are possible by integrating a few clinical parameters available at the bedside. For instance, including the administered noradrenaline dose as an additional input improved the AUROC for sepsis prediction from 0.80 (95 % CI [0.76; 0.84]) to 0.87 (95 % CI [0.83; 0.90]). We want to emphasise, however, that incorporating clinical data may introduce biases and limit generalisability. For example, treatment choices such as the administered noradrenaline dose depend on the implementation of clinical guidelines, which are subject to variation over time and across health systems.

While we showed that the HSI + clinical data models largely outperformed widely used

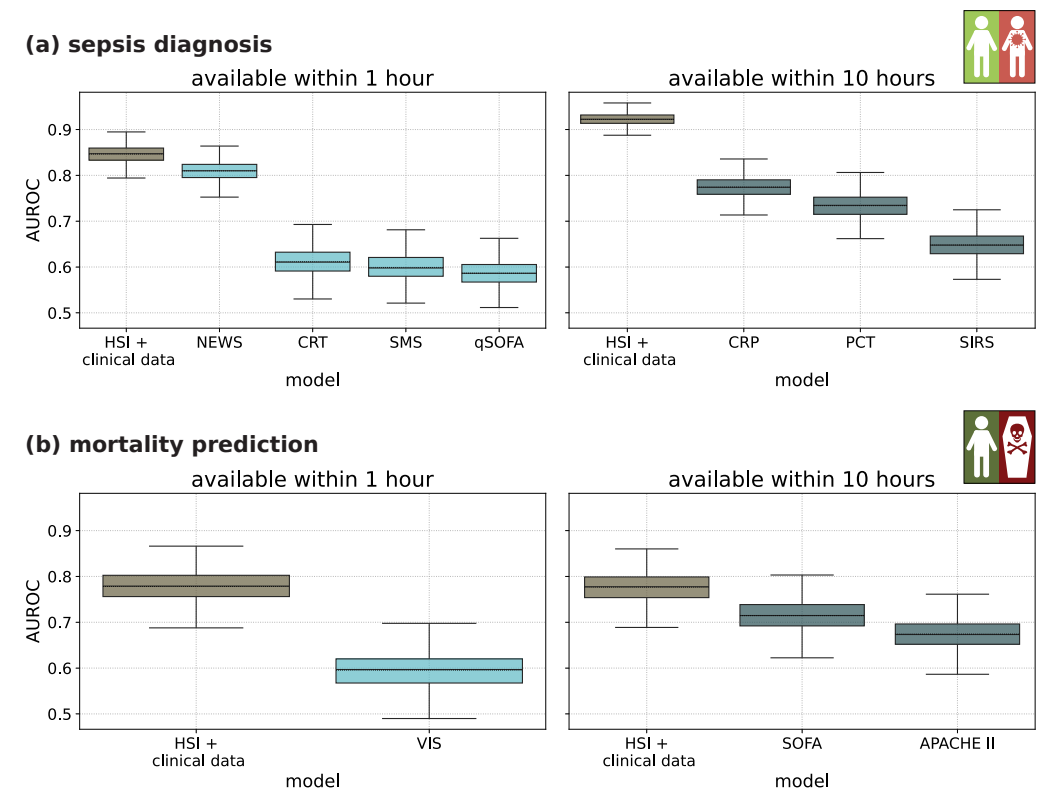


Fig. 5 Our hyperspectral imaging (HSI) biomarker outperforms widely used clinical biomarkers and scores for sepsis diagnosis and mortality prediction. Comparison of the area under the receiver operating characteristic curve (AUROC) for deep learning-based sepsis diagnosis (a) and mortality prediction (b) using HSI and clinical data against clinical biomarkers and scores. For data available within one hour of intensive care unit admission (left), the comparison includes National Early Warning Score (NEWS), capillary refill time (CRT), skin mottling score (SMS), quick Sequential Organ Failure Assessment (qSOFA) score, and vasoactive inotropic score (VIS). For data available within ten hours of admission (right), the comparison includes C-reactive protein (CRP), procalcitonin (PCT), Systemic Inflammatory Response Syndrome (SIRS) criteria, Sequential Organ Failure Assessment (SOFA) score, and Acute Physiology and Chronic Health Evaluation (APACHE) II score. Each box plot displays the quartiles of the AUROC distribution across 1000 bootstrap samples, with whiskers extending up to 1.5 times the interquartile range. The median and mean are represented by solid and dashed lines, respectively.

clinical biomarkers and scores and achieved excellent sepsis diagnosis and mortality prediction performance, another limitation of models that require clinical data is that prospectively collecting clinical data requires substantial labour. We decided against the less labour-intensive export of EHR data, as several clinical parameters are not reliably recorded in the EHR, which would lead to inaccuracies. Additionally, many clinical parameters, such as vital signs and ventilation parameters, were stored in the EHR at a poor temporal resolution, failing to accurately reflect the patient's status at the time of HSI measurement. Given the labour-intensive collection of clinical data, minimising the number of clinical parameters required for prediction is advantageous. Our

results demonstrate that our HSI + clinical data models outperform clinical data models for both sepsis diagnosis and mortality prediction when only few clinical parameters are available.

3.2 Comparison to the state of the

Previous research has explored characteristic patterns in tissue functional parameters derived from HSI when comparing septic patients to healthy volunteers [24, 25], as well as septic non-survivors to survivors [26]. Recent initial work on HSI-based sepsis diagnosis by ourselves [27] and others [28] showed promising early results for differentiating between sepsis patients and healthy volunteers or

selectively chosen cohorts, such as patients undergoing pancreatic surgeries. Due to the presence of potential confounders in these studies (e.g., age gaps, differences in comorbidities and therapies between septic patients and non-septic controls), the algorithms risk shortcut learning and are unlikely to generalise well to realistic clinical applications, such as automated sepsis diagnosis in critically ill ICU patients. This hypothesis is supported by the difference in our sepsis diagnosis performance in ICU patients, where we achieved an AUROC of 0.80, compared to the higher AUROC of 0.92 reported for differentiating between sepsis patients and healthy volunteers in [28]. Automated sepsis diagnosis and mortality prediction in ICU patients is particularly challenging due to high baseline illness severity and frequent organ failure from both septic and non-septic inflammation.

Despite the shortcomings in the selection of a clinically relevant control group in previous work, as well as the use of different HSI systems, and methods to compute tissue functional parameters, some of the characteristic patterns that we identified for sepsis patients and non-survivors are in agreement with findings in previous work:

- We found significantly lower tissue oxygen saturation in septic patients and non-survivors, in accordance with [24–26]. This finding is also in agreement with the current knowledge of sepsis pathophysiology, in which tissue hypoxia was identified as a key driver of organ dysfunction [39].
- We observed significantly higher tissue water content in sepsis patients and non-survivors, in agreement with [24]. The increase in tissue water content could on the one hand be explained by the formation of edema due to capillary leakage, a pathomechanism in sepsis that promotes the extravasation of fluid into interstitial space [40]. On the other hand, fluid administration, crucial in sepsis treatment, risks fluid overload that could also contribute to the formation of edema and development of organ damage [41].
- Tissue haemoglobin content was significantly increased in septic patients and non-survivors,

in agreement with [24]. This could be a consequence of the sepsis microcirculatory dysfunction, potentially resulting in areas of stagnant blood flow [42].

We could not confirm a significant drop in perfusion for septic patients, that was previously described in [24] in comparison to healthy volunteers.

3.3 Future work

A key limitation of our study is that all data were collected from a single surgical ICU in Germany. External validation is required to confirm the generalizability of our HSI biomarker across different ICUs and study populations. Furthermore, given the key strengths of our HSI biomarker, which enables a rapid, non-invasive, cost-effective, and mobile assessment of sepsis diagnosis and mortality, investigating its performance in resource-constrained and time-critical settings, such as ambulances, emergency wards, and LMICs, is a promising future direction. Additionally, since an estimated 40% of sepsis cases in 2017 occurred in children under 5 years old [2], expanding the cohort to include infants is of interest.

While we consider our single time-point measurements advantageous for enabling immediate diagnosis and low resource requirements, studies collecting longitudinal HSI data could expand the potential of HSI biomarkers. For example, the current therapeutic target in shock therapy is macrohaemodynamic stabilisation (e.g., maintaining normative arterial blood pressure), but critically ill patients, particularly those with sepsis, often experience a loss of haemodynamic coherence, resulting in dissociation between macro- and microcirculation [43]. While no other widely available clinical data can capture the spatial distribution of tissue microcirculation, HSI biomarkers may offer novel therapeutic strategies by evaluating the effects of the implemented therapy on the tissue microcirculation and guiding treatment. Additionally, longitudinally acquired HSI data could enhance understanding of features related to disease improvement or worsening.

3.4 Conclusion

In this study, we addressed the critical need for reliable biomarkers to identify septic patients and those at high risk of mortality. We are the first to investigate the potential of HSI for sepsis diagnosis and mortality prediction in ICU patients, based on a prospective study with the largest HSI patient cohort to date, involving over 480 patients. Our proposed HSI biomarkers demonstrated high predictive performance, which improved further when combined with minimal clinical data. They outperformed widely used clinical biomarkers and scores. Key strengths of HSI biomarkers include their rapid, non-invasive, cost-effective, and mobile measurements, making them promising candidates for various clinical settings, including resource-limited scenarios (e.g., LMICs) and time-critical situations (e.g., ambulances, emergency wards). Beyond their proven benefit in sepsis diagnosis and mortality prediction, HSI-based microcirculatory monitoring could also offer novel therapeutic strategies and enhance understanding of disease progression. Our code and pretrained models will be made publicly available.

4 Methods

Study design

HSI data was collected at the Heidelberg University Hospital following approval by the Ethics Committee of the Medical Faculty of Heidelberg University, Germany (study reference number: S-288/2022). Measurements were performed on all adult patients at admission to the interdisciplinary surgical ICU, over a period of one year. HSI cubes of the patients' skin at the palm and annular finger measurement sites were acquired, ensuring the selected hand was not used for intra-arterial cannula or intravascular access. Simultaneously, clinical data were collected, including demographics, vital signs, blood gas analysis measurements, therapy details (usage of organ replacement therapies, ventilation parameters, dose of administered vasopressors and inotropes), and laboratory results. In total, 45 clinical parameters were recorded. Of these, 33 were available within one hour of admission, while the 12 laboratory parameters were available within ten hours of admission. Table A2 and Table A3 provide descriptive statistics of the clinical data.

Hyperspectral image acquisition

The camera system used was the medical device-graded TIVITA® 2.0 Surgery Edition (Diaspective Vision GmbH, Am Salzhaff, Germany). It features a push-broom design with a spectral resolution of approximately 5 nm, covering 100 spectral channels in the range of 500 nm to 1000 nm. The resulting HSI cubes have dimensions of $640 \times 480 \times 100$ (width × height × number of spectral channels). The imaged area is approximately 16×11.5 cm, with an imaging distance of about 50 cm, maintained by an integrated distance calibration system. Image acquisition takes approximately 7 s.

The system includes both an HSI and RGB sensor, providing simultaneous RGB images with dimensions of $640 \times 480 \times 3$ (width \times height \times number of channels). Tissue parameter images, such as oxygen saturation, perfusion index, haemoglobin index, and water index, are estimated from the HSI data according to the formulas published in [29].

During image acquisition, window blinds were lowered, and all light sources other than the integrated light-emitting diode (LED) unit were turned off. The hands of patients were supported by the examiner to prevent motion artefacts and ensure more uniform hand positioning, with a consistent background used across all images.

Hyperspectral image annotation

Despite using a uniform background and standardising hand positioning as much as possible, images might still include elements such as dressings, wounds, wires, tubes, or parts of the examiner's gloved hand. To mitigate potential confounding from these elements, our analysis was performed on annotated skin areas. We chose circular annotations to consistently capture the same measurement sites across patients, regardless of hand rotation in the imaging plane. According to our annotation guidelines, the selected annotation radii were 100 pixels for the palm and 20 pixels for the ring finger. Finger annotations were centred on the fingertip, and palm annotations were centred on the palm of the hand, defined as the area enclosed by the wrist, the metacarpophalangeal joints and the thumb basal joint.

Sepsis and outcome labels

Diagnosis of sepsis was based on the Sepsis-3 criteria, which define it as acute, life-threatening organ dysfunction resulting from a suspected or confirmed infection [1]. Organ dysfunction was evaluated using the SOFA score, with an acute increase of at least two points indicating sepsis. Differentiating between organ failure caused by sepsis and that resulting from non-septic inflammation can be challenging, particularly in a surgical ICU setting following surgical trauma. To maintain label quality and avoid ambiguity in such cases, we introduced a third label, "unsure", alongside the labels "sepsis" and "no sepsis". For each patient, the sepsis status was independently assessed by two expert anaesthetists. Disagreements between the two anaesthetists were resolved by a third, more senior anaesthetist (the head of the department for anaesthesia and intensive care). Mortality was assessed through a follow-up conducted 30 days after the patient's inclusion.

Data statistics

Initially, 508 patients were included in the study. Thereof, 71 patients were excluded from training and validation of the sepsis diagnosis model because their sepsis status was unsure. Of the remaining 437 patients, 129 (30 %) were diagnosed with sepsis, while 308 (70 %) were not. Among septic patients, the majority (53 %) had an abdominal focus, followed by 17 % with a respiratory focus, 5 % with a skin or soft tissue focus, and 3 % with a genitourinary focus. Additionally, 8 % had multiple foci.

For training and validation of the mortality prediction model, 25 patients were excluded due to unsuccessful follow-up. Among the remaining 483 patients, 68 (14%) died within 30 days of inclusion. The mortality rate was higher among patients with sepsis at the time of admission, at 27% (35/129), compared to 6% (18/308) for those without sepsis at admission.

Data preprocessing

Following calibration of HSI cubes using white and dark reference cubes, ℓ^1 -normalisation was applied across the spectral channels. Both HSI and RGB cubes were cropped to a square that tightly encompassed the circular annotation, with pixels outside the annotated area set to zero.

The cropped cubes were rescaled to dimensions of $224 \times 224 \times 100$ and $224 \times 224 \times 3$, respectively (width \times height \times number of spectral channels). The missingness in the clinical parameters was low, averaging at 1.6%. Missing values were imputed with -1.

$Classification\ models$

Deep learning classifiers were utilised for the HSI and HSI + clinical data models. For classification based on clinical data, a random forest classifier was employed, as it is commonly used in related work on sepsis diagnosis from EHR data [11].

The HSI model is composed of a ResNet14d [44, 45] architecture with pre-trained ImageNet weights.

The HSI + clinical data model consists of two submodels: The HSI data is processed equivalently to the HSI model by a ResNet14d model with pre-trained ImageNet weights up to the bottleneck layer. The clinical data is handled by a submodel comprising two fully connected blocks. Each block includes a linear, batch normalisation, exponential linear unit activation, and dropout layer. The linear layer in the first block has a size of 50, while a size of 30 was set in the second block. The two blocks are followed by a linear head of size ten, matching the bottleneck layer size of the HSI submodel. After batch normalisation of both bottleneck layers, the bottleneck features are concatenated and fed into another fully connected block, followed by the final classification head.

For both the HSI and HSI + clinical data models, cross entropy loss was used during training. The same hyperparameter settings were applied across all deep learning models. Data augmentations included rotations up to $\pm 180^{\circ}$, and horizontal and vertical flipping, each with a probability of 0.5. The AdamW optimizer [46] and an exponential learning rate schedule were used (initial learning rate: 0.001, decay rate γ : 0.99, Adam decay rates β_1 : 0.9 and β_2 : 0.999). To regularise the network, a weight decay of 0.001 was applied. Training was conducted for ten epochs, each consisting of 500 images, with stochastic weight averaging [47] applied over the last two epochs. A batch size of 32 images was used, and underrepresented classes were oversampled in each batch to ensure equal class distribution.

The clinical data model is a random forest classifier consisting of 100 trees. The implementation from sklearn [48] was used with default settings, except that balanced class weighting was enabled to adjust the weights inversely proportional to the class frequencies in the training data.

Training and validation setup

The same training and validation setup was used across all trained models. Given the limited dataset size, we decided against a single hold-out test set for model validation. Instead, we implemented a nested cross-validation scheme, providing a more robust performance estimation based on the entire dataset [49]. Both the number of outer and inner folds were set to five.

To further stabilise the performance of the trained networks, each run was repeated three times with different random seed settings, altering the initialization of workers and the order in which images were seen during training. On the validation sets, ensembling was performed over these three repetitions. For the test data, the networks from all five folds and three repetitions each (a total of 15 networks) were ensembled by averaging the predictions (logits).

Following the recommendations in [50], the model performances were validated using the receiver operating characteristic (ROC) curve and AUROC. To compute confidence intervals that reflect sampling variability, bootstrap sampling was repeated 1000 times for each test set T, with |T| samples randomly drawn with replacement for each bootstrap.

Feature importance of clinical data

The feature importance of the clinical data was determined using recursive feature elimination (RFE) [51] from the random forest models. RFE was adapted to the 5-fold cross-validation setup of our inner folds by averaging feature importances across inner folds before eliminating the least important feature from the set of input features. This process was performed independently on all five outer folds.

Statistical testing

Statistical tests were conducted to identify significant differences in functional tissue parameter

values between septic and non-septic patients, as well as between survivors and non-survivors, resulting in four tests for each group. Two-sided Welch's t-test [52] was applied, with an overall significance level of 0.05 for each group of tests. To prevent the accumulation of alpha errors due to multiple testing, the Bonferroni correction [53] was applied, setting the significance level at 0.0125 per test.

Reporting summary

Further information on research design is available in the Nature Research Reporting Summary linked to this article.

Declarations

Data availability

The data supporting the results in this study are available within the paper. The raw patient data is not available, as consent for study participation and data sharing was not obtained from the patients, in accordance with the ethics approval. However, to nevertheless enable model comparison and external validation, all pretrained models will be made publicly available in our GitHub repository https://github.com/IMSY-DKFZ/htc [54].

Code availability

All code will be made publicly available in our GitHub repository https://github.com/IMSY-DKFZ/htc [54].

References

- Singer, M. et al. The Third International Consensus Definitions for Sepsis and Septic Shock (Sepsis-3). JAMA 315, 801–810 (2016).
- [2] Rudd, K. E. et al. Global, regional, and national sepsis incidence and mortality, 1990– 2017: analysis for the global burden of disease study. The Lancet 395, 200–211 (2020).
- [3] Ferrer, R. et al. Empiric antibiotic treatment reduces mortality in severe sepsis and septic shock from the first hour: results from a guideline-based performance improvement program. Critical care medicine 42, 1749–1755 (2014).

- [4] Vincent, J.-L. (ed.). Annual Update in Intensive Care and Emergency Medicine 2023. Annual Update in Intensive Care and Emergency Medicine (Springer Nature Switzerland, 2023).
- [5] Henning, D. J. et al. The absence of fever is associated with higher mortality and decreased antibiotic and iv fluid administration in emergency department patients with suspected septic shock. Critical care medicine 45, e575–e582 (2017).
- [6] Choi, M. H. et al. Mortality prediction of patients in intensive care units using machine learning algorithms based on electronic health records. Scientific reports 12, 7180 (2022).
- [7] Kumar, A. A. Mortality prediction in the icu: The daunting task of predicting the unpredictable. *Indian J Crit Care Med* **26**, 13–14 (2022).
- [8] Iwase, S. *et al.* Prediction algorithm for icu mortality and length of stay using machine learning. *Scientific reports* **12**, 12912 (2022).
- [9] Pierrakos, C., Velissaris, D., Bisdorff, M., Marshall, J. C. & Vincent, J.-L. Biomarkers of sepsis: time for a reappraisal. *Critical Care* 24, 1–15 (2020).
- [10] Komorowski, M., Green, A., Tatham, K. C., Seymour, C. & Antcliffe, D. Sepsis biomarkers and diagnostic tools with a focus on machine learning. EBioMedicine 86 (2022).
- [11] Yang, Z., Cui, X. & Song, Z. Predicting sepsis onset in icu using machine learning models: a systematic review and meta-analysis. *BMC infectious diseases* **23**, 635 (2023).
- [12] Fleuren, L. M. et al. Machine learning for the prediction of sepsis: a systematic review and meta-analysis of diagnostic test accuracy. Intensive care medicine 46, 383–400 (2020).
- [13] Islam, K. R. et al. Machine learning-based early prediction of sepsis using electronic health records: A systematic review. Journal of clinical medicine 12, 5658 (2023).

- [14] Sauer, C. M. et al. Leveraging electronic health records for data science: common pitfalls and how to avoid them. The Lancet Digital Health 4, e893–e898 (2022).
- [15] Wong, A. et al. External validation of a widely implemented proprietary sepsis prediction model in hospitalized patients. JAMA internal medicine 181, 1065–1070 (2021).
- [16] Moor, M. et al. Predicting sepsis using deep learning across international sites: a retrospective development and validation study. EClinicalMedicine 62 (2023).
- [17] Woldemariam, M. T. & Jimma, W. Adoption of electronic health record systems to enhance the quality of healthcare in low-income countries: a systematic review. *BMJ Health & Care Informatics* **30** (2023).
- [18] Wang, H., Ding, H., Wang, Z.-Y. & Zhang, K. Research progress on microcirculatory disorders in septic shock: A narrative review. *Medicine* 103, e37273 (2024).
- [19] Raia, L. & Zafrani, L. Endothelial activation and microcirculatory disorders in sepsis. Frontiers in Medicine 9, 907992 (2022).
- [20] Walley, K. Heterogeneity of oxygen delivery impairs oxygen extraction by peripheral tissues: theory. *Journal of applied physiology* 81, 885–894 (1996).
- [21] Østergaard, L. et al. Microcirculatory dysfunction and tissue oxygenation in critical illness. Acta Anaesthesiologica Scandinavica 59, 1246–1259 (2015).
- [22] De Backer, D. et al. Microcirculatory alterations in patients with severe sepsis: impact of time of assessment and relationship with outcome. Critical care medicine 41, 791–799 (2013).
- [23] Trzeciak, S. et al. Early microcirculatory perfusion derangements in patients with severe sepsis and septic shock: relationship to hemodynamics, oxygen transport, and survival.

 Annals of emergency medicine 49, 88–98 (2007).

- [24] Dietrich, M. et al. Bedside hyperspectral imaging indicates a microcirculatory sepsis pattern an observational study. Microvascular Research 136 (2021).
- [25] Lācis, M., Kazune, S., Marcinkevics, Z., Rubins, U. & Grabovskis, A. Hahlweg, C. F. & Mulley, J. R. (eds) Hybrid optical prototype for sepsis bedside diagnostics. (eds Hahlweg, C. F. & Mulley, J. R.) Novel Optical Systems, Methods, and Applications XXII, Vol. 11105, 111050P. International Society for Optics and Photonics (SPIE, 2019).
- [26] Kazune, S. et al. Relationship of mottling score, skin microcirculatory perfusion indices and biomarkers of endothelial dysfunction in patients with septic shock: an observational study. Critical Care 23, 1–9 (2019).
- [27] Dietrich, M. et al. Machine learning-based analysis of hyperspectral images for automated sepsis diagnosis. arXiv preprint arXiv:2106.08445 (2021).
- [28] Kohnke, J. et al. A proof of concept for microcirculation monitoring using machine learning based hyperspectral imaging in critically ill patients: a monocentric observational study. Critical Care 28, 230 (2024).
- [29] Holmer, A., Marotz, J., Wahl, P., Dau, M. & Kämmerer, P. W. Hyperspectral imaging in perfusion and wound diagnostics methods and algorithms for the determination of tissue parameters. *Biomedical Engineering / Biomedizinische Technik* 63, 547–556 (2018).
- [30] Kulcke, A. et al. A compact hyperspectral camera for measurement of perfusion parameters in medicine. Biomedical Engineering / Biomedizinische Technik 63, 519–527 (2018).
- [31] Ait-Oufella, H. et al. Mottling score predicts survival in septic shock. Intensive care medicine 37, 801–807 (2011).
- [32] Pan, P., Su, L., Liu, D. & Wang, X. Microcirculation-guided protection strategy in hemodynamic therapy. Clinical Hemorheology and Microcirculation 75, 243–253 (2020).

- [33] National early warning score (news): standardising the assessment of acute-illness severity in the nhs. Report of working party. London: Royal College of Physicians (2012).
- [34] Bone, R. C. *et al.* Definitions for sepsis and organ failure and guidelines for the use of innovative therapies in sepsis. *Chest* **101**, 1644–1655 (1992).
- [35] Gaies, M. G. et al. Vasoactive—inotropic score as a predictor of morbidity and mortality in infants after cardiopulmonary bypass. Pediatric critical care medicine 11, 234–238 (2010).
- [36] Knaus, W. A., Draper, E. A., Wagner, D. P. & Zimmerman, J. E. Apache ii: a severity of disease classification system. *Critical care medicine* 13, 818–829 (1985).
- [37] Yoon, J. Hyperspectral imaging for clinical applications. *BioChip Journal* **16**, 1–12 (2022).
- [38] Bartlett, E. S. et al. Critical care delivery across health care systems in low-income and low-middle-income country settings: A systematic review. Journal of Global Health 13 (2023).
- [39] Arora, J., Mendelson, A. A. & Fox-Robichaud, A. Sepsis: network pathophysiology and implications for early diagnosis. American Journal of Physiology-Regulatory, Integrative and Comparative Physiology 324, R613–R624 (2023).
- [40] McMullan, R. R., McAuley, D. F., O'Kane, C. M. & Silversides, J. A. Vascular leak in sepsis: physiological basis and potential therapeutic advances. *Critical Care* 28, 97 (2024).
- [41] Malbrain, M. L. et al. Principles of fluid management and stewardship in septic shock: it is time to consider the four d's and the four phases of fluid therapy. Annals of intensive care 8, 1–16 (2018).
- [42] Pool, R., Gomez, H. & Kellum, J. A. Mechanisms of organ dysfunction in sepsis. *Critical*

- care clinics 34, 63-80 (2018).
- [43] Ince, C. Hemodynamic coherence and the rationale for monitoring the microcirculation. *Critical care* **19**, S8 (2015).
- [44] He, K., Zhang, X., Ren, S. & Sun, J. Deep residual learning for image recognition. 2016 IEEE Conference on Computer Vision and Pattern Recognition (CVPR) 770-778 (2016).
- [45] Wightman, R. Pytorch image models (2019).
- [46] Loshchilov, I. & Hutter, F. Decoupled weight decay regularization. arXiv preprint arXiv:1711.05101 (2019).
- [47] Izmailov, P., Podoprikhin, D., Garipov, T., Vetrov, D. & Wilson, A. G. Averaging weights leads to wider optima and better generalization. arXiv preprint arXiv:1803.05407 (2018).
- [48] Pedregosa, F. et al. Scikit-learn: Machine learning in Python. Journal of Machine Learning Research 12, 2825–2830 (2011).
- [49] Varma, S. & Simon, R. Bias in error estimation when using cross-validation for model selection. *BMC bioinformatics* **7**, 1–8 (2006).
- [50] Maier-Hein, L. et al. Metrics reloaded: recommendations for image analysis validation. Nature Methods 21, 195–212 (2024).
- [51] Guyon, I., Weston, J., Barnhill, S. & Vapnik, V. Gene selection for cancer classification using support vector machines. *Machine learning* 46, 389–422 (2002).
- [52] Welch, B. L. The generalization of 'student's'problem when several different population variances are involved. *Biometrika* 34, 28–35 (1947).
- [53] Bonferroni, C. E. Il calcolo delle assicurazioni su gruppi di teste. Studi in onore del professore salvatore ortu carboni 13–60 (1935).
- [54] Sellner, J. & Seidlitz, S. Hyperspectral tissue classification (2024). URL https://github.com/IMSY-DKFZ/htc.

Acknowledgements

This project has received funding from the European Research Council (ERC) under the European Union's Horizon 2020 research and innovation programme (project NEURAL SPICING grant agreement No. 101002198) and the National Center for Tumor Diseases (NCT) Heidelberg's Surgical Oncology Program. It was further supported by the German Cancer Research Center (DKFZ) and the Helmholtz Association under the joint research school HIDSS4Health (Helmholtz Information and Data Science School for Health). This publication was supported through state funds approved by the State Parliament of Baden-Württemberg for the Innovation Campus Health + Life Science alliance Heidelberg Mannheim. The European Society of Anaesthesiology and Intensive Care (ESAIC) supported the project with the ESAIC Andreas Hoeft's Grant Intensive Care in 2023 (Grant ID: ESAIC_GR_2023_MD). Lena Maier-Hein worked with the medical device manufacturer KARL STORZ SE & Co. KG in the projects "InnOPlan" and "OP 4.1", funded by the German Federal Ministry of Economic Affairs and Energy (grant agreement No. BMWI 01MD15002E and BMWI 01MT17001E) and "Surgomics", funded by the German Federal Ministry of Health (grant agreement No. BMG 2520DAT82D).

Author contributions

MD, MAW, LMH and SS conceived and designed the study. LMH, MD and MAW acquired the funding. KH and AvG collected and annotated the data. MD, TH, SK, MvdF and MAW labelled the data. SS and JS performed the analysis. SS wrote the manuscript. LMH, JS, MAW and MD revised the manuscript. All authors have read and approved the final manuscript.

Competing interests

Authors state no conflict of interest.

Acronyms

APACHE Acute Physiology and Chronic Health Evaluation

AUROC area under the receiver operating characteristic curve

CI confidence interval

CRP C-reactive protein

CRT capillary refill time

EHR electronic health record

HSI hyperspectral imaging

ICU intensive care unit

 $\it LED$ light-emitting diode

LMICs low- and middle-income countries

NEWS National Early Warning Score

PCT procalcitonin

qSOFAquick Sequential Organ Failure Assessment

RFE recursive feature elimination

RGB red-green-blue

ROC receiver operating characteristic

SIRS Systemic Inflammatory Response Syndrome

SMS skin mottling score

SOFA Sequential Organ Failure Assessment

 $V\!I\!S$ vasoactive inotropic score

Appendix A Extended data

target	functional parameter	p-value	DOF	$t ext{-statistic}$	95% CI
sepsis status sepsis status sepsis status	oxygen saturation perfusion index haemoglobin index	$7.1 \cdot 10^{-4} \\ 1.1 \cdot 10^{-1} \\ 6.2 \cdot 10^{-5}$	208 205 198	-3.44 -1.63 4.09	$ \begin{bmatrix} -0.06; -0.02 \\ -0.03; 0.00 \\ \hline [0.03; 0.08] $
sepsis status survival status survival status survival status survival status	water index oxygen saturation perfusion index haemoglobin index water index	$4.5 \cdot 10^{-10}$ $6.8 \cdot 10^{-4}$ $2.5 \cdot 10^{-3}$ $6.0 \cdot 10^{-4}$ $7.0 \cdot 10^{-5}$	222 79 82 81 93	6.53 -3.54 -3.12 3.57 4.16	$ \begin{bmatrix} 0.03; 0.06 \\ -0.09; -0.02 \\ -0.06; -0.01 \\ 0.03; 0.09 \\ 0.02; 0.05 \end{bmatrix} $

Table $\overline{\mathbf{A1}}$ Statistical tests were performed to determine significant differences in functional tissue parameter values based on sepsis status and survival status. A summary of p-values, degrees of freedom (DOF), t-statistic and 95 % confidence interval (CI) is provided.

attribute	no sepsis	sepsis	non survivor	survivor				
number of subjects	308	129 demographics	68	415				
age sex	$6.2 \cdot 10^{1} (1.5 \cdot 10^{1})$ 220 male 88 female	$6.6 \cdot 10^{1} (1.4 \cdot 10^{1})$ 90 male 39 female	$6.9 \cdot 10^{1} (1.5 \cdot 10^{1})$ 41 male 27 female	$6.3 \cdot 10^{1} (1.4 \cdot 10^{1})$ 299 male 116 female				
weight [kg] type of weight measurement	$8.2 \cdot 10^{1} (2.0 \cdot 10^{1})$ 245 estimated 53 measured	$8.2 \cdot 10^1 (2.6 \cdot 10^1)$ 100 estimated 16 measured vital signs	$7.5 \cdot 10^1 (2.3 \cdot 10^1)$ 52 estimated 8 measured	$8.2 \cdot 10^{1} (2.1 \cdot 10^{1})$ 331 estimated 68 measured				
heart frequency [bpm]	$8.2 \cdot 10^1 \ (1.7 \cdot 10^1)$	$9.9 \cdot 10^1 \ (2.1 \cdot 10^1)$	$9.8 \cdot 10^1 \ (2.4 \cdot 10^1)$	$8.6 \cdot 10^1 \ (1.9 \cdot 10^1)$				
sinusrhythm [%] MAP [mmHg] systolic blood pressure	$79 8.1 \cdot 10^{1} (1.4 \cdot 10^{1}) 1.2 \cdot 10^{2} (2.3 \cdot 10^{1})$	$74 7.6 \cdot 10^{1} (1.3 \cdot 10^{1}) 1.2 \cdot 10^{2} (1.9 \cdot 10^{1})$	$ 60 7.7 \cdot 10^1 \ (1.3 \cdot 10^1) 1.2 \cdot 10^2 \ (2.3 \cdot 10^1) $	$78 8.0 \cdot 10^{1} (1.4 \cdot 10^{1}) 1.2 \cdot 10^{2} (2.3 \cdot 10^{1})$				
temperature [°C] SpO2 [%]	$3.7 \cdot 10^{1} (6.7 \cdot 10^{-1}) 9.7 \cdot 10^{1} (2.2)$	$3.7 \cdot 10^{1} (1.1)$ $9.7 \cdot 10^{1} (4.0)$ BGA measurements	$ 3.7 \cdot 10^{1} (1.1) 9.6 \cdot 10^{1} (5.1) $	$3.7 \cdot 10^{1} \ (7.5 \cdot 10^{-1}) 9.7 \cdot 10^{1} \ (2.3)$				
pCO2 [mmHg] pO2 [mmHg] sO2 [%] Hb (BGA) [g dL ⁻¹]	$\begin{array}{c} 3.9 \cdot 10^1 \; (5.8) \\ 9.8 \cdot 10^1 \; (3.4 \cdot 10^1) \\ 9.7 \cdot 10^1 \; (1.6) \\ 9.7 \; (1.7) \end{array}$	$\begin{array}{c} 4.4 \cdot 10^1 \ (9.8) \\ 1.0 \cdot 10^2 \ (2.5 \cdot 10^1) \\ 9.6 \cdot 10^1 \ (2.8) \\ 9.4 \ (1.7) \end{array}$	$\begin{array}{c} 4.3 \cdot 10^1 \ (9.8) \\ 1.0 \cdot 10^2 \ (2.5 \cdot 10^1) \\ 9.6 \cdot 10^1 \ (3.5) \\ 9.5 \ (1.6) \end{array}$	$\begin{array}{c} 4.0 \cdot 10^1 \ (7.0) \\ 9.9 \cdot 10^1 \ (3.2 \cdot 10^1) \\ 9.7 \cdot 10^1 \ (1.6) \\ 9.5 \ (1.7) \end{array}$				
lactate $[mg dL^{-1}]$ pH type BGA	$1.6 \cdot 10^{1} \ (1.4 \cdot 10^{1})$ $7.4 \ (5.8 \cdot 10^{-2})$ $274 \ \text{arterial}$ $7 \ \text{venous}$	$2.7 \cdot 10^{1} (3.4 \cdot 10^{1})$ $7.4 (8.8 \cdot 10^{-2})$ 104 arterial 1 venous	$\begin{array}{c} 4.6 \cdot 10^{1} \ (5.3 \cdot 10^{1}) \\ 7.4 \ (1.0 \cdot 10^{-1}) \\ 56 \ \text{arterial} \end{array}$	$1.5 \cdot 10^{1} \ (1.1 \cdot 10^{1})$ $7.4 \ (6.5 \cdot 10^{-2})$ $358 \ \text{arterial}$ $10 \ \text{venous}$				
non al nonla comont		gan replacement there		7				
renal replacement therapy $[\%]$	4	20	28	7				
ECMO [%] impella [%] liver replacement therapy [%]	1 0 1	2 1 2	3 4 4	1 0 0				
10 []		ventilation paramete	rs					
invasive ventilation [%]	48	95	93	59				
ventilation [%] APRV [%] FiO2 [%] PEEP [mbar] P-peak [mbar] respiratory frequency [min ⁻¹]	$\begin{array}{c} 23 \\ 0 \\ 3.2 \cdot 10^{1} \ (1.0 \cdot 10^{1}) \\ 7.0 \ (2.3) \\ 2.0 \cdot 10^{1} \ (5.5) \\ 1.7 \cdot 10^{1} \ (4.4) \end{array}$	$\begin{array}{c} 80 \\ 2 \\ 4.4 \cdot 10^{1} \ (1.8 \cdot 10^{1}) \\ 8.9 \ (3.2) \\ 2.1 \cdot 10^{1} \ (6.1) \\ 1.8 \cdot 10^{1} \ (5.3) \end{array}$	$ 78 3 4.4 \cdot 10^{1} (1.7 \cdot 10^{1}) 8.3 (3.3) 2.2 \cdot 10^{1} (5.7) 1.7 \cdot 10^{1} (5.6) $	$\begin{array}{c} 34 \\ 0 \\ 3.4 \cdot 10^{1} \ (1.3 \cdot 10^{1}) \\ 8.1 \ (2.9) \\ 2.0 \cdot 10^{1} \ (5.8) \\ 1.7 \cdot 10^{1} \ (5.0) \end{array}$				
	dose of administered vasopressors and inotropes							
noradrenaline dose $[\mu g kg^{-1} min^{-1}]$	$4.4 \cdot 10^{-2} \ (9.4 \cdot 10^{-2})$	$2.6 \cdot 10^{-1} \ (2.6 \cdot 10^{-1})$	$2.7 \cdot 10^{-1} \ (3.0 \cdot 10^{-1})$	$7.7 \cdot 10^{-2} \ (1.4 \cdot 10^{-1})$				
adrenaline dose $[\mu g kg^{-1} min^{-1}]$	$9.2 \cdot 10^{-4} \ (1.1 \cdot 10^{-2})$	$3.7 \cdot 10^{-3} \ (2.3 \cdot 10^{-2})$	$8.6 \cdot 10^{-3} \ (3.2 \cdot 10^{-2})$	$7.0 \cdot 10^{-4} \ (1.0 \cdot 10^{-2})$				
vasopressin dose $[\text{Unit kg}^{-1} \text{min}^{-1}]$	$3.8 \cdot 10^{-6} \ (3.2 \cdot 10^{-5})$	$5.4 \cdot 10^{-5} \ (1.4 \cdot 10^{-4})$	$5.2 \cdot 10^{-5} \ (1.1 \cdot 10^{-4})$	$1.2 \cdot 10^{-5} \ (7.3 \cdot 10^{-5})$				
dobutamine dose $[\mu g kg^{-1} min^{-1}]$	$2.0 \cdot 10^{-1} \ (9.3 \cdot 10^{-1})$	$6.1 \cdot 10^{-1} \ (1.9)$	1.1 (2.4)	$2.7 \cdot 10^{-1} \ (1.2)$				

Table A2 Descriptive statistics are provided for patients with and without sepsis, as well as for survivors and non-survivors. This includes clinical data available within the first hour of admission to the intensive care unit (ICU), such as demographics, vital signs, blood gas analysis (BGA) measurements, use of organ replacement therapies, ventilation parameters, and dose of administered vasopressors and inotropes. For ratio-scaled parameters, means are presented with standard deviation (SD) in brackets. For nominal-scaled parameters, the number of patients per category is listed, while for boolean therapy parameters, the percentage of patients receiving the treatment is provided. Abbreviations denote the mean arterial pressure (MAP), pulse oxymetrical oxygen saturation (SpO2), carbon dioxide partial pressure (pCO2), oxygen partial pressure (pO2), oxygen saturation (sO2), haemoglobin concentration (Hb), extracorporeal membrane oxygenation (ECMO), airway pressure release ventilation (APRV), fraction of inspired oxygen (FiO2), positive endexpiratory pressure (PEEP), and peak inspiratory pressure (P-peak).

attribute	no sepsis	sepsis	non survivor	survivor
creatinine $[\operatorname{mg} dL^{-1}]$	1.3 (1.1)	1.9 (1.5)	$1.7 \ (9.7 \cdot 10^{-1})$	1.5 (1.3)
GFR [mL min ⁻¹]	$7.3 \cdot 10^1 \ (3.6 \cdot 10^1)$	$4.9 \cdot 10^1 \ (3.4 \cdot 10^1)$	$4.6 \cdot 10^1 \ (2.9 \cdot 10^1)$	$6.7 \cdot 10^1 \ (3.7 \cdot 10^1)$
$LDH \left[Unit L^{-1} \right]$	$5.4 \cdot 10^2 \ (7.8 \cdot 10^2)$	$6.8 \cdot 10^2 \ (1.6 \cdot 10^3)$	$1.3 \cdot 10^3 \ (2.3 \cdot 10^3)$	$4.8 \cdot 10^2 \; (6.7 \cdot 10^2)$
bilirubin	1.9 (2.4)	2.4 (3.5)	2.7 (3.7)	1.9(2.4)
$[\operatorname{mg} dL^{-1}]$	1 . 1.	0 . 0.	0 . 1.	0 . 0.
$CRP \left[mg L^{-1} \right]$	$6.6 \cdot 10^1 \ (7.4 \cdot 10^1)$	$2.0 \cdot 10^2 \ (1.1 \cdot 10^2)$	$1.2 \cdot 10^2 \ (9.5 \cdot 10^1)$	$1.1 \cdot 10^2 \ (1.1 \cdot 10^2)$
leukocytes [nL ⁻¹]	$1.1 \cdot 10^1 \ (5.0)$	$1.6 \cdot 10^1 \ (1.1 \cdot 10^1)$	$1.5 \cdot 10^1 \ (9.7)$	$1.3 \cdot 10^1 \ (7.3)$
Hb (lab) $[\mathrm{g}\mathrm{d}\mathrm{L}^{-1}]$	9.9 (1.9)	9.8 (1.8)	9.6 (1.6)	9.8 (1.9)
platelets $[nL^{-1}]$	$1.6 \cdot 10^2 \ (8.3 \cdot 10^1)$	$2.1 \cdot 10^2 \ (1.4 \cdot 10^2)$	$1.8 \cdot 10^2 \ (1.2 \cdot 10^2)$	$1.8 \cdot 10^2 \ (1.1 \cdot 10^2)$
hematocrit [%]	$2.9 \cdot 10^{-1} \ (5.3 \cdot 10^{-2})$	$3.0 \cdot 10^{-1} \ (5.5 \cdot 10^{-2})$	$2.9 \cdot 10^{-1} \ (5.1 \cdot 10^{-2})$	$2.9 \cdot 10^{-1} \ (5.4 \cdot 10^{-2})$
sodium $[\text{mmol } L^{-1}]$	$1.4 \cdot 10^2 \ (4.3)$	$1.4 \cdot 10^2 \ (6.0)$	$1.4 \cdot 10^2 \ (5.9)$	$1.4 \cdot 10^2 \ (4.9)$
potassium	$4.5 (5.3 \cdot 10^{-1})$	$4.7 (6.2 \cdot 10^{-1})$	$4.7 (6.8 \cdot 10^{-1})$	$4.5 (5.4 \cdot 10^{-1})$
$[\text{mmol L}^{-1}]$,	•	,	, , ,
$PCT [ng mL^{-1}]$	1.9 (7.7)	$5.2 \cdot 10^1 \ (1.6 \cdot 10^2)$	$2.3 \cdot 10^1 \ (6.3 \cdot 10^1)$	$1.6 \cdot 10^1 \ (9.6 \cdot 10^1)$

Table A3 Continuation of Table A2, including descriptive statistics for laboratory parameters available within the first ten hours of admission to the intensive care unit (ICU). Means are presented with standard deviation (SD) in brackets. Abbreviations denote the glomerular filtration rate (GFR), lactate dehydrogenase (LDH), C-reactive protein (CRP), haemoglobin concentration (Hb), and procalcitonin (PCT)